Available online at www.sciencedirect.com
SCIENCE DIRECT®
International Journal of Solids and Structures 43 (2006) 1308–1330
INTERNATIONAL JOURNAL OF SOLIDS and STRUCTURES
www.elsevier.com/locate/ijsolstr

Stiffness of planar tensegrity truss topologies

Bram de Jager [a,*], Robert E. Skelton [b,1]

[a] Department of Mechanical Engineering, Technische Universiteit Eindhoven, P.O. Box 513, 5600 MB Eindhoven, The Netherlands
[b] Department of Mechanical and Aerospace Engineering, University of California at San Diego, La Jolla, CA 92093-0411, USA

Received 15 November 2004; received in revised form 5 June 2005
Available online 15 August 2005

Abstract

This paper proposes and demonstrates a symbolic procedure to compute the stiffness of truss structures built up from simple basic units. Geometrical design parameters enter in this computation. A set of equations linear in the degrees-of-freedom, but nonlinear in the design parameters, is solved symbolically in its entirety. The resulting expressions reveal the values of the design parameters which yield desirable properties for the stiffness or stiffness-to-mass ratio. By enumerating a set of topologies, including the number of basic units, and a set of material distribution models, stiffness properties are optimized over these sets. This procedure is applied to a planar tensegrity truss. The results make it possible to optimize the structure with respect to stiffness properties, not only by appropriately selecting (continuous) design parameters like geometric dimensions, but also by selecting an appropriate topology for the structure, e.g., the number of basic units, and a material distribution model, all of which are discrete design decisions.
© 2005 Elsevier Ltd. All rights reserved.

Keywords: Geometry; Material distribution; Optimization; Stiffness; Symbolic analysis; Tensegrity; Topology; Truss structure

1. Introduction

As a step in integrating system design in system theory (Skelton, 2002), we consider a powerful class of mechanical systems, namely tensegrity structures, that are relatively easy to analyze, and so permit analytical solutions, even for large structures when build up systematically from basic units. Tensegrities are used as landmarks (Klimke et al., 2004), as art objects (Snelson, 1996), as architectural identities (Liapi and Kim, 2004), as cell models (Ingber, 2003), as engineering structures (Fest et al., 2003), and more.

* Corresponding author. Fax: +31 40 2461418.
E-mail addresses: a.g.de.jager@wfw.wtb.tue.nl (B. de Jager), bobskelton@ucsd.edu (R.E. Skelton).
[1] Fax: +1 858 3107/822 3107.

0020-7683/$ - see front matter © 2005 Elsevier Ltd. All rights reserved.
doi:10.1016/j.ijsolstr.2005.06.049

Tensegrity structures are defined here as truss structures (so with ball joints) consisting of two pre-assigned types of members, tensile ones (tendons) and compressive ones (bars), and allowing a state of pre-stress. See Motro and Raducanu (2003) for alternative definitions. The truss class of structures has been studied for a long time, see, e.g., Maxwell (Forew, 1890), whose terminology consisted of ties and struts instead of tendons and bars.

When members are pre-stressed sufficiently, an external load does not cause a reverse in load directions in any member, facilitating a linear analysis. Hence, in tensegrities, tendons are exclusively loaded in tension, otherwise they would buckle because they are normally very slender. Bars are generally loaded in compression only, and not in tension. Tensegrity structures can be divided into different classes, depending on the number of bars connecting in a node. In the sequel we consider class 1 and class 2 and 3 tensegrities. For a more extensive introduction and overview of recent work in modeling of tensegrities see Skelton et al. (2002), and for deployment of tensegrities see Sultan and Skelton (2003).

The main advantage of tensegrity systems is that an equilibrium is possible in different configurations or shapes, by adjusting the rest length of the tensile (or compressive) members. This can be done by "active" members. In general these equilibria can be made equipotential, making it easy, energy wise, to go from one equilibrium to another, and so from one shape to another. Using only small amounts of energy is possible, also in the presence of pre-stress, by making use of techniques like those outlined in Scruggs and Iwan (2003), which enables the transfer of energy from one member to another, efficiently. Another advantage of tensegrities is the assigned role for compressive and tensile members, which holds for all load conditions, allowing a choice of specialized material to be made during the design.

Tendons can function as sensor or as actuator or both. Alternatively, bars can be used as actuators or sensors. By controlling the length of all tendons simultaneously, a tensegrity structure can be made very stiff for any static load acting on the nodal points. It is not always feasible to equip all tendons as actuators, so the stiffness properties inherent to the structure are still important. Because those properties depend on topology, geometry, and material distribution, it is of interest to study their influences.

Our main goal is to obtain guidelines in the design of planar tensegrity structures of different classes. Structural aspects studied are changes in stiffness and stiffness-to-mass ratio due to variations in topology, geometry, and material distribution. This work is an extension to other topologies (both class 1 and class 2 and 3) and to other discrete design decisions of the work reported in De Jager and Skelton (2004).

Other works related to structural design of tensegrities include the computation of tensegrity equilibria (Williamson et al., 2003; Bayat and Crane III, 2004), the stability of tensegrity structures (Connelly and Back, 1998), and the influence and optimization of pre-stress (Hanaor, 1988; Pellegrino, 1990). For optimization of structures, besides the method discussed in this paper, the free material design method in Bendsøe (1989, 1995) can be mentioned because this is useful for topology optimization. Truss optimization via elimination from a ground structure, using an extensive number of members on a grid, e.g., (Ben-Tal and Nemirovski, 1997; Jarre et al., 1998), can be mentioned because also here topological design decisions are possible, due to member elimination. Tensegrity optimization via a numeric approach is worked out in Masic (2004). Building up complete structures from basic units is possible with repetitive structures, (Noor, 1988; Karpov et al., 2002; Guest and Hutchinson, 2003; Babuška and Sauter, 2004), as will be done here. However, we will not make use of the (approximate) simplified analysis of repetitive structures with a discrete field approach or as a continuum (Noor, 1988). Another way of building structures from elementary units is hierarchical, which is the main subject of hierarchical structure analysis and design (Ashby, 1991; Lakes, 1993; Murphey and Hinkle, 2003; McEachen et al., 2004). From these contributions it appears that hierarchical structures can be very beneficial, in that they make improvements of orders of magnitude possible in structural properties.

Our approach deviates from the design methods above in being analytic, so exact, in the spirit of Noor and Andersen (1979), Leff and Yun (1991), Pavlović (2003) or of Oppenheim and Williams (2000). It considers several design aspects—topology, geometry, material distribution—in a unified way. Due to

computational complexity, the contribution is restricted to the easily analyzed class of truss structures, with a restricted geometric parameterization and with simple material distribution models, but allows for a large number of members, which is unusual for an analytic approach.

This contribution is organized as follows. We first discuss several aspects of modeling tensegrity systems of class 1 and higher. This is followed by a discussion of how we determine the stiffness of the structure symbolically, as a function of a small set of geometric design parameters. Then the computational results are given and discussed, and guidelines for the design of tensegrities are formulated.

2. Planar tensegrity structures

A tensegrity structure consists of bars and tendons, arranged in a stable equilibrium, so it is not a mechanism. This is achieved by choosing topology and geometry appropriately, and by pre-stressing the tendons. A planar tensegrity structure is one that only extends in the plane. A tensegrity structure can be of class 1, where bars are only connected by tendons, and do not connect directly, or of class 2, where up to two bars and a number of tendons are connected in a nodal point. This can be generalized to a class k definition (Williamson et al., 2003). Often a tensegrity structure is made up of nested or repeated tensegrity structures, giving it a fractal (Skelton et al., 2002) or repetitive character. This is beneficial for analysis and design, because only a limited number of structures needs to be investigated. Those structures can then be used to build up a more complex structure.

2.1. Description of planar tensegrity structures

An elementary or basic unit, numbered i, of a planar tensegrity structure of class 1 is given in Fig. 1. This unit consists of 2 bars and 10 tendons, all indicated with the upper index i. It can be repeated indefinitely, by replicating it, shifted some distance of the horizontal dimension, to build up a planar structure in x-direction. It could also be replicated in y-direction or in both.

The connection of the unit is indicated in Fig. 1 by the node numbers. To node numbers with upper index $i-1$ the bars from the unit to the left side are attached, while nodes with upper index $i+1$ belong to the bars of the unit that attaches from the right.

Without diagonal tendons structural stiffness is derived from second order effects (i.e., it is zero in the linear approximation, except for pre-stress, in other words, an infinitesimal mechanism would be present), so diagonal tendons are included. In essence, we consider a ''class I pre-stressable'' structure, according to the definition in Hanaor (1988), or a ''redundant'' structure, according to Murakami and Nishimura (2001).

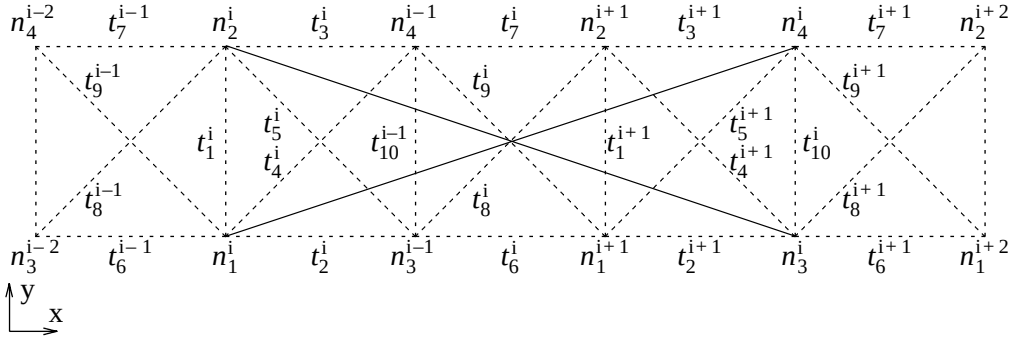

Fig. 1. Single unit of planar tensegrity structure; —: bars of unit i, --: tendons of units $i-1$, i, $i+1$.

The left side of the structure is modified for the boundary condition. The left side removes the three DOF (degrees-of-freedom) of the rigid body, in effect, it restricts movement of the upper left node in both x and y-coordinate direction, i.e., the node is translationally fixed, and of the lower left node in the x-direction.

There are no restrictions specified at the right side. Only differences in boundary conditions are taken into account: the connection of some tendons is to different nodes than in Fig. 1 because there is no other unit that attaches from the right.

The setup of the structure in Fig. 1 already specifies the topology, i.e., the connectivity of bars and tendons. In this case the units are shifted with respect to each other over a relatively large distance. When the shift is smaller, so the units overlap over a longer distance, node n_4^{i-1} and n_2^{i+1} will cross over and tendons that connect to these nodes need to be connected to different nodes to assure a suitable tensegrity structure. This gives a different topology. The geometry is determined by the nodal positions.

2.2. Model of planar tensegrities

The basic assumptions in setting up the model are the same as in De Jager and Skelton (2004). They can be summarized as being the standard assumptions for linear analysis of trusses, e.g., only elongation and no bending of the members, due to revolute joints, straight members, and nodal forces only, while the displacements are kept small. Additionally, the bars are assumed to be inelastic. When this additional assumption is appropriate for a truss, the results are also of value for standard truss design.

The symbolic model is derived for a planar tensegrity system, as seen in Fig. 2 for a 3-unit structure, with a minimal number of tendons still allowing a state of pre-stress, so compared to Fig. 1 the "inner" vertical tendons and the "uneven" pairs of diagonal tendons are removed. Only the horizontal, the left and right vertical tendons, and the diagonal tendons that cross the overlap are included in the model. Including diagonal tendons eliminates infinitesimal mechanisms (Pellegrino and Calladine, 1986; Hanaor, 1988).

The equilibrium conditions for small perturbations u of the DOF are used to derive a set of equations that is linear in these perturbations, so

$$K(\theta)u = w, \tag{1}$$

with K the symbolic stiffness matrix that depends on topology, on material distribution, and on a vector θ of geometric parameters, and with w the nodal force vector. The influence of pre-stress on stiffness is ignored.

The matrix K is sparse and only the area around the diagonal is normally filled, making it easier to solve the set of linear equations, not only numerically, but also symbolically. Loading the structure at a specific node with a force F and computing the corresponding deflection y will then give insight in the stiffness and stiffness-to-mass properties of the structure. For setting up $K(\theta)$ use is made of length ratios, in this case between the length of a line perpendicular to the horizontal or vertical (e.g., the length of t_1^i in Fig. 1) and the length of the hypothenusa (e.g., the distance between n_2^i and n_3^i in Fig. 1), to avoid trigonometric

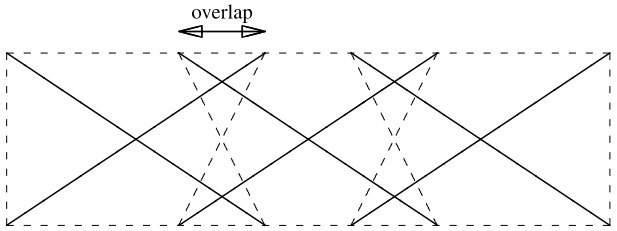

Fig. 2. Tensegrity with minimal number of tendons; —: bars, --: tendons.

terms (direction cosines) in $K(\theta)$, and so to simplify the symbolic computations. More details about setting up $K(\theta)$ are available in De Jager and Skelton (2004).

Given a topology and material distribution, the goal is to optimize the geometry, characterized by the overlap between the units of a multi-unit tensegrity structure and by the angles of the bars. The optimization should be repeated for several topologies and material distributions. The optimum depends on the stiffness of the tendons, on the number of units and the way the tendons are connected, on the overlap, and on the slenderness of the structure. The overlap and the number of units determine the appropriate tendon connectivity. The number of units, overlap, and slenderness together determine the bar angle, so that is not an independent design variable.

To get an "easy" parameterization, overlap and slenderness are used as geometric parameters. To analyze the effect of the number of units we have to enumerate, the same holds for different tendon connectivities and material distribution models. We limit the number of design parameters to get a structure that is easy to manufacture, all units are identical, except for boundary conditions, and to make symbolic computation possible for systems with a large number of units, say hundred or more.

The set of equilibrium equations can be solved symbolically,

$$u(\theta) = K(\theta)^{-1} w, \tag{2}$$

because the equations are linear in the unknown u, and the parameter dependency can be parameterized polynomially when over-parameterization is used, i.e., three instead of two geometric parameters. Using the length of the diagonal members as additional design parameter avoids the use of square roots in the expressions, that would stall the computations at a smaller number of units of the structure than desired.

Given the analytical solution for the displacements u, as functions of the design parameters, the additional design parameter can be eliminated by substitution of the relation between the three geometric parameters. It is then straightforward to obtain values for the overlap and slenderness that minimize the displacement of a specific point of the structure for a given load at the nodal points, or to obtain values that optimize the stiffness or stiffness-to-mass ratio. This can be done by symbolic differentiation, establishing stationary points,

$$\frac{\partial u(\theta)}{\partial \theta_i} = 0, \tag{3}$$

and solving the resulting equation for the design parameters θ_i.

3. Stiffness and stiffness-to-mass ratio

To characterize a large class of geometries the two design parameters are non-dimensionalized, so the slenderness ratio $l = l_x/l_y$, with l_x and l_y the horizontal and vertical dimensions of the structure, and the overlap factor s in the overlap $h = sl_x$ between units are used. The overlap h is the distance between the right nodes of unit i and the left nodes of unit $i+1$, see Fig. 2. Note that s is made dimensionless by the horizontal length of the complete structure and not by the length of a single unit. We could also have chosen the non-dimensionalization $h = \bar{s} l_u$ for the overlap, with l_u the horizontal length of a single unit. The relations between s and $\bar{s}$ are

$$\bar{s} = \frac{ns}{(n-1)s+1}, \quad s = \frac{\bar{s}}{n-(n-1)\bar{s}}, \tag{4}$$

with n the number of units. The main reason to choose s in θ, and not $\bar{s}$, is that the horizontal length of a unit,

$$l_u = \frac{(n-1)s+1}{n} l l_y, \tag{5}$$

is an affine function in s, while it is a nonlinear function in $\bar{s}$. Thus, when using $\bar{s}$ as element of the parameter vector θ, the terms with parameters in $K(\theta)$ are more complicated than when s is used. So using s is preferred for the computation of the deflection. It may be more instructive to represent the results using $\bar{s}$, however.

The parameters s and l will be varied in characterizing the solutions. The external force F at a node and the stiffness factor k of the tendons always appear in the combination F/k in the deflection y, due to the linear analysis. In the stiffness the force F drops out and k appears affinely, see (7).

For the stiffness-to-mass ratio the mass of the bars, M_b, is computed assuming a constant cross-sectional area, A_b, and the same specific mass, ρ, for all bars. The mass of the bars is then proportional to their lengths, l_b, and can be expressed as a function of l_y, l, s, and n, where l_y appears affinely, by

$$M_b = 2\rho A_b l_y \sqrt{((n-1)s+1)^2 l^2 + n^2}. \tag{6}$$

The tendon lengths depend on s, etc., also, but need to be computed taking the topology into account.

Only for $0 < s < 1/(n+1)$ is the topology in Fig. 2 a valid one, except for $n = 2$ where $0 < s < 1$ holds. For $n = 3$ and $1/4 < s < 1$ we change the topology and get a so-called super tensegrity cross, see Fig. 3. With every step in n an additional topology becomes available, due to an increase in the number of units that can be covered by the overlap. We do not consider these additional topologies for $n > 3$.

For $n = 3$ there are three other topologies, giving a total of 5, that are of interest, namely for $s = 0$, $s = 1/4$, and $s = 1$, where some nodal points can be "pinned" together to get a class 2 or class 3 tensegrity. For every step in n an additional pinned topology becomes available, due to an additional transition between unpinned topologies. We only consider the pinned topologies for $n = 3$.

For pinned nodes, we do not reformulate the model to a reduced set of DOF, but we use (additional) tendons whose stiffness goes to ∞ in the limit, causing the nodes to be pinned. Due to the analytical procedure followed, the limiting process is exact. In the sequel we report results for the five topologies of $n = 3$. The techniques developed can be used for larger n, where the number of different topologies increases. We will present results for larger n, however, only for the class 1 tendon connectivity in Fig. 3.

For the stiffness of the tendons three models are explored. The constitutive relations still represent linear elastic material, because we restrict ourselves to a linear analysis, so the stiffness models are really material distribution models. The models are:

1. Stiffness $k_i = EA_i/l_i = k$ is constant and the same for all tendons. Here E is the modulus of elasticity, A_i the cross-sectional area of tendon i, and l_i its length. Note that the material is distributed proportional to the length squared of the tendons because A_i has to be proportional to tendon length l_i to make the stiffness constant.

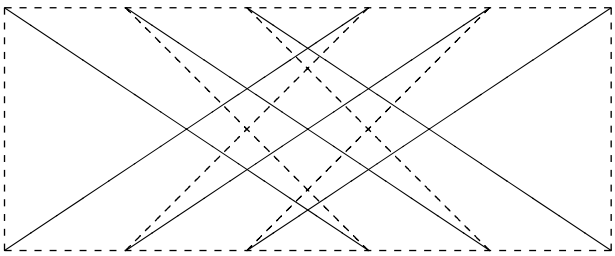

Fig. 3. Super tensegrity cross; —: bars, --: tendons.

2. Stiffness is $k_i = EA/l_i$, with A the cross-sectional area of the tendons. Note that all tendons have the same cross-sectional area A in this model, so material is distributed proportional to tendon length.
3. Stiffness is $k_i = EV/l_i^2$, with V the volume of a tendon. Note that all tendons have the same volume V in this model, so material is distributed independent of tendon length.

The second model is probably the most relevant one, it assumes that tendons are made from the same material with the same cross-sectional area, so the structure is easy to manufacture. In truss optimization sometimes the volume of the members is varied, see, e.g., the approach in Jarre et al. (1998), to get low compliance for fixed mass, but this leads to solutions were most members need a different cross-sectional area, which complicates the manufacturing process. Here, this complication also occurs for material distribution models 1 and 3, although at most five different cross-sectional area's will be used, which could also be an additional constraint in a numeric approach. Models 1 and 3 are included to check the influence of differences in material distribution.

The approaches for truss optimization mentioned above are also hampered by the fact that they assume a fixed grid, while here the overlap, and so the nodal positions, can be varied continuously and nodes are not tied to a fixed grid. This can be done in a numeric approach also, see Ben-Tal et al. (1993) or Masic (2004). The computation becomes more involved, however.

Instead of using the same k, EA, or EV for all tendons, they can also be set for tendons individually, taking symmetry into account. This is indicated in Fig. 4, where k_i, $i = 0, \ldots, 4$, indicate the standard tendons (minimal set still allowing pre-stress), and k_5 and k_6 indicate some additional tendons, that are in principal superfluous for making the structure pre-stressable, but that are used to compute the stiffness when nodes are pinned to obtain a class 2 or 3 tensegrity. These tendons will also make for a larger set of configurations (positions of nodal points) for which a static equilibrium with pre-stress in all tendons is possible. A disadvantage of including tendons with a larger reach is that the stiffness matrix K is not as sparse and diagonally concentrated anymore, so the symbolic computations are only viable for small values of n.

For optimizing the geometry we use a single load condition and three design criteria. The load is a vertical force F at the top/right node and y is the corresponding vertical deflection of this node. This is bending for a cantilever type construction. As explained in Murphey and Hinkle (2003), bending of a cantilever type construction is a typical load scenario that can also be seen as representing other loads, and is therefore suited to compare different structural designs.

The first criterion is the stiffness of the structure regarded as a beam, F/y, the ratio of force and displacement of the top/right node. For the second criterion the stiffness is normalized by the dimensionless volume, V_t, of the tendon material used, $N = F/y/V_t$. The tendon volume depends on the tendon stiffness model and the number and/or lengths of the individual tendons. The third criterion is the normalized stiffness-to-mass ratio, N/M_b. The criteria are normally scaled to allow for easy comparison.

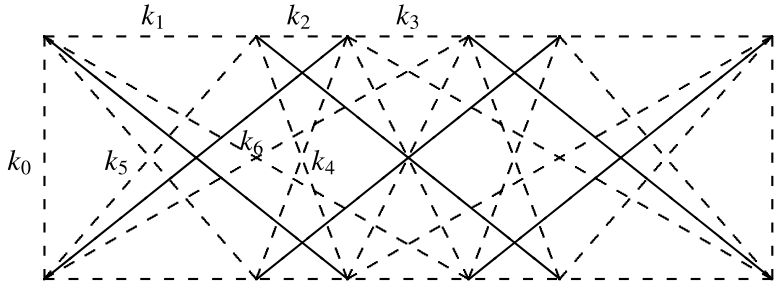

Fig. 4. Tensegrity with individual tendon stiffnesses; —: bars, --: tendons.

The relations for the stiffness are proportional to k, EA, or EV and inversely proportional to various powers of l_y, depending on the stiffness model, and further have a "polynomial" denominator (including powers of square roots) in s and l. These relations are differentiated with respect to s, to obtain stationary, and so optimal, points by equating them to zero. The resulting algebraic relation can be solved for s analytically, but only when the degree of the polynomial is not too large, or when the polynomial can be factored in lower order polynomials. In general this solution is quite complex for polynomials of degree 3 and larger, and representing the solution in graphical form is preferred.

4. Results for structural analysis

We present the stiffness, normalized stiffness, and normalized stiffness-to-mass ratio results for several cases:

- uniform and individual tendon stiffnesses,
- class 1 and class 2 or 3 structures,
- three tendon stiffness models.

4.1. Stiffness formulae

The stiffness results are first given for class 1 tensegrities, both for uniform and individual tendons stiffness models, and then for class 2 tensegrities.

4.1.1. Uniform tendon stiffness models

To present concise expressions for stiffness, define

$$\frac{F}{y} = k^{\alpha} S_{\beta}^{\alpha}, \tag{7}$$

where k^{α} with $\alpha = 1, 2, 3$ is the tendon stiffness according to the definitions in Section 3 where l_y is used as characteristic length, so $k^1 = k$, $k^2 = EA/l_y$, and $k^3 = EV/l_y^2$, while $\beta = 1$ for the class 1 topology of Fig. 2 and $\beta = 2$ for the class 1 topology of Fig. 3. Then the dimensionless expressions for S_2^{α} for $n = 3$ are as follows (for S_1^{α} see De Jager and Skelton, 2004):

$$S_2^1 = \frac{18}{28l^2s^2 - 20l^2s + 55l^2 + 27}, \tag{8}$$

$$S_2^2 = \frac{54}{-10l^3s^3 + 54(l^2s^2 + 1)^{3/2} + 30l^3s^2 - 30l^3s + 37l^3 + 27}, \tag{9}$$

$$S_2^3 = \frac{162}{172l^4s^4 - 40l^4s^3 + 240l^4s^2 + 324l^2s^2 - 184l^4s + 55l^4 + 243}. \tag{10}$$

The results for normalized stiffness are given by dividing the expressions for S_{β}^{α} by the non-dimensional volume of the tendons. The normalized stiffness-to-mass results are obtained by dividing the expressions for the normalized stiffness by the non-dimensional mass of the bars, m_n, which for $n = 3$ is

$$m_n = 2\sqrt{4l^2s^2 + 4l^2s + l^2 + 9}, \tag{11}$$

while the mass itself is $M_b = \rho A l_y m_n$.

For other values of n the structure and degree of the polynomials in S are the same, only the coefficients change. Despite the remark in Pavlović (2003) that "Obviously, pure symbolic equation-solving in the FEM

is restricted to systems with few simultaneous linear equations", followed by mentioning a dozen equations as "few", here systems that are more than 100 times as large (>1500) have been solved. This is due to four key features.

1. The complexity of the final result (structure and degree of the polynomials) is independent of n, a feature of the problem.
2. The matrix $K(\theta)$ is sparse and non-zero entries are concentrated around the main diagonal, due to careful ordering of elements of u and w.
3. The geometric parameterization is simple, due to the choice of s instead of $\bar{s}$ and due to overparameterization.
4. The expressions in the entries of K are non-trigonometric, due to the avoidance of direction cosines.

These features limit the intermediate expression swell to manageable proportions. Seemingly trivial changes to the set-up may destroy this property, see also Pavlović (2003).

The coefficients for values of n other than 3 and for topology 2 are in Tables 1–3, where the coefficients are defined as below:

$$S_2^1 = \frac{a}{b_{22}l^2s^2 + b_{21}l^2s + b_{20}l^2 + b_{00}}, \tag{12}$$

$$S_2^2 = \frac{a}{b_{33}l^3s^3 + b_{3/2}(l^2s^2+1)^{3/2} + b_{32}l^3s^2 + b_{31}l^3s + b_{30}l^3 + b_{00}}, \tag{13}$$

$$S_2^3 = \frac{a}{b_{44}l^4s^4 + b_{43}l^4s^3 + b_{42}l^4s^2 + b_{22}l^2s^2 + b_{41}l^4s + b_{40}l^4 + b_{00}}. \tag{14}$$

Table 1
Parameters for stiffness model 1

n	a	b_{22}	b_{21}	b_{20}	b_{00}
1	2	0	0	1	1
2	4	3	−2	7	4
4	8	19	−14	35	16
8	16	91	−70	155	64
16	32	395	−310	651	256
32	64	1643	−1302	2667	1024
64	128	6699	−5334	10,795	4096
128	256	27,051	−21,590	43,435	16,384
256	512	108,715	−86,870	174,251	65,536

Table 2
Parameters for stiffness model 2

n	a	b_{33}	$b_{3/2}$	b_{32}	b_{31}	b_{30}	b_{00}
1	2	0	0	0	0	1	1
2	8	−1	4	3	−3	5	4
4	16	−2	24	7	−8	11	8
8	256	15	896	15	−75	173	128
16	2048	381	15,360	−415	−313	1371	1024
32	16,384	4217	253,952	−5691	−1269	10,935	8192
64	131,072	38,641	4,128,768	−55,411	−5101	87,407	65,536
128	1,048,576	329,185	66,584,567	−483,555	−20,445	699,103	524,288

Table 3
Parameters for stiffness model 3

n	a	b_{44}	b_{43}	b_{42}	b_{22}	b_{41}	b_{40}	b_{00}
1	2	0	0	0	0	0	1	1
2	16	9	−4	18	16	−12	5	16
4	128	211	−56	422	384	−240	47	256
8	512	2407	−1430	5000	3584	−1514	145	2048
16	16,384	185,343	−135,556	348,690	245,760	−57,236	2823	131,072
32	262,144	6,460,801	−5,008,276	11,302,838	8,126,464	−983,732	24,849	4,194,304
64	4,194,304	215,253,253	−170,055,988	360,930,686	264,241,152	−16,266,100	208,421	134,217,728

For topology 1 the coefficients can be found in De Jager and Skelton (2004). The results presented are given for powers of 2, but can be computed for any positive $n \in \mathbb{N}$ if n is not too large, say $n < 256$, depending on topology and stiffness model. It is possible to get expressions for $n \to \infty$, but not by explicit computation, so all limiting cases (s is 0 or 1, l is 0 or ∞, and n is 3 or ∞) can be treated. The techniques needed for the case $n \to \infty$ fall outside the scope of this contribution, however.

4.1.2. Individual tendon stiffness models

When the tendon stiffness is individually assigned (with account of symmetry) the following results are obtained, where S_β^α now includes the individual tendon stiffness factors $k_0, \ldots, k_4$, (see Fig. 4) replacing the factors k, EA, and EV of the three stiffness models, so S is no longer non-dimensional. Effectively, S_β^α from (7) is now replaced by

$$\frac{F}{y} = k^\alpha S_\beta^\alpha, \tag{15}$$

with $k^1 = 1$, $k^2 = 1/l_y$, and $k^3 = 1/l_y^2$. The results in Section 4.1.1 can be obtained by setting all k_i's in the following expressions equal to 1:

$$\frac{1}{S_1^1} = \left(\frac{4}{9}\frac{l^2}{k_1} + \frac{1}{9}\frac{l^2}{k_2} + \frac{l^2}{k_4}\right)s^2 - \left(\frac{8}{9}\frac{l^2}{k_1} + \frac{2}{9}\frac{l^2}{k_2}\right)s + \frac{13}{9}\frac{l^2}{k_1} + \frac{10}{9}\frac{l^2}{k_2} + \frac{1}{2}\frac{l^2}{k_3} + \frac{1}{2}\frac{1}{k_0} + \frac{1}{k_4}, \tag{16}$$

$$S_2^1 = S_1^1, \tag{17}$$

$$\frac{1}{S_1^2} = -\left(\frac{4}{27}\frac{l^3}{k_1} - \frac{1}{9}\frac{l^3}{k_2}\right)s^3 + \frac{(l^2s^2+1)^{3/2}}{k_4} + \left(\frac{4}{9}\frac{l^3}{k_1} - \frac{2}{9}\frac{l^3}{k_2}\right)s^2 - \left(\frac{7}{9}\frac{l^3}{k_1} - \frac{10}{9}\frac{l^3}{k_2} + \frac{2}{3}\frac{l^3}{k_3}\right)s + \frac{13}{27}\frac{l^3}{k_1} + \frac{1}{6}\frac{l^3}{k_3} + \frac{1}{2}\frac{1}{k_0}, \tag{18}$$

$$\frac{1}{S_2^2} = -\left(\frac{4}{27}\frac{l^3}{k_1} + \frac{1}{27}\frac{l^3}{k_2}\right)s^3 + \frac{(l^2s^2+1)^{3/2}}{k_4} + \left(\frac{4}{9}\frac{l^3}{k_1} + \frac{1}{9}\frac{l^3}{k_2}\right)s^2 - \left(\frac{7}{9}\frac{l^3}{k_1} + \frac{4}{9}\frac{l^3}{k_2} - \frac{2}{3}\frac{l^3}{k_3}\right)s + \frac{13}{27}\frac{l^3}{k_1} + \frac{10}{27}\frac{l^3}{k_2} - \frac{1}{6}\frac{l^3}{k_3} + \frac{1}{2}\frac{1}{k_0}, \tag{19}$$

$$\frac{1}{S_1^3} = \left(\frac{4}{81}\frac{l^4}{k_1} + \frac{1}{9}\frac{l^4}{k_2} + \frac{l^4}{k_4}\right)s^4 - \left(\frac{16}{81}\frac{l^4}{k_1} + \frac{2}{9}\frac{l^4}{k_2}\right)s^3 + \left(\frac{11}{27}\frac{l^4}{k_1} + \frac{10}{9}\frac{l^4}{k_2} + \frac{8}{9}\frac{l^4}{k_3}\right)s^2 + 2\frac{l^2}{k_4}s^2 - \left(\frac{34}{81}\frac{l^4}{k_1} + \frac{4}{9}\frac{l^4}{k_3}\right)s + \frac{13}{81}\frac{l^4}{k_1} + \frac{1}{18}\frac{l^4}{k_3} + \frac{1}{2}\frac{1}{k_0} + \frac{1}{k_4}, \tag{20}$$

$$\frac{1}{S_2^3} = \left(\frac{4}{81}\frac{l^4}{k_1} + \frac{1}{81}\frac{l^4}{k_2} + \frac{l^4}{k_4}\right)s^4 - \left(\frac{16}{81}\frac{l^4}{k_1} + \frac{4}{81}\frac{l^4}{k_2}\right)s^3 + \left(\frac{11}{27}\frac{l^4}{k_1} + \frac{5}{27}\frac{l^4}{k_2} + \frac{8}{9}\frac{l^4}{k_3}\right)s^2 + 2\frac{l^2}{k_4}s^2 - \left(\frac{34}{81}\frac{l^4}{k_1} + \frac{22}{81}\frac{l^4}{k_2} + \frac{4}{9}\frac{l^4}{k_3}\right)s + \frac{13}{81}\frac{l^4}{k_1} + \frac{10}{81}\frac{l^4}{k_2} + \frac{1}{18}\frac{l^4}{k_3} + \frac{1}{2}\frac{1}{k_0} + \frac{1}{k_4}. \tag{21}$$

Normalized stiffness and normalized stiffness-to-mass ratio are computed in the same way as in Section 4.1.1.

It is easy to see that for stiffness models 2 and 3, when $s = 0$, k_2 does not appear in the stiffness formulae (topology 1), when $s = 1/4$, k_3 does not appear (topology 1 and 2), and when $s = 1$, k_1 and k_2 do not appear (topology 2), because the length of the corresponding tendons goes to 0, so their stiffness goes to ∞. To obtain the effect of eliminating tendons whose length goes to 0 when using stiffness model 1, the limit should be taken for the corresponding tendon stiffness going to ∞.

4.1.3. Class 2 and 3 tensegrities

The stiffening effect described in Section 4.1.2 is not sufficient to pin the nodes, due to the linearized set of equations. Tendons of zero length are only infinitely stiff (for stiffness models 2 and 3) in the direction of the tendon vector, not perpendicular to the vector (neglecting pre-stress and second-order effects).

To completely pin nodes that are on top of each other, and so compute the stiffness of class 2 tensegrities, additional tendons are used, those labeled with k_5 and k_6 in Fig. 4. For the special case $s = 0$, $k_5 \to \infty$, for $s = 1/4$, $k_6 \to \infty$, and for $s = 1$, $k_4 \to \infty$, so the limit of the stiffness of these tendons to ∞ is taken to completely pin nodes that are on top of each other. For stiffness model 1, additionally, for $s = 0$, $k_2 \to \infty$, for $s = 1/4$, $k_3 \to \infty$, and for $s = 1$, $k_1 \to \infty$ and $k_2 \to \infty$, to stiffen tendons that become of zero length and so pin the nodes.

The limiting process is done symbolically to get exact results. It does not add additional stiffness to the structure, besides pinning common nodes, because for these specific values of s those rigidized tendons are aligned with bars that are already infinitely stiff. For all other values of s the stiffness of tendons labeled with k_5 or k_6 is taken equal to 0. Due to the additional tendons used to pin joints, structures with pinned joints have a stiffness that is larger or equal than the corresponding structures, so with the same value of s, without pinned joints. The results for stiffness for $n = 3$ are given below for the uniform tendon stiffness models, while Table 4 gives the results for the factor of improvement achieved by pinning for the limiting values of l.

For $s = 0$ we get

$$S^1 = 18\frac{4l^2 + 27}{140l^4 + 981l^2 + 81}, \tag{22}$$

$$S^2 = 54\frac{4l^3 + 81}{140l^6 + 2943l^3 + 729}, \tag{23}$$

$$S^3 = 162\frac{4l^4 + 243}{140l^8 + 8829l^4 + 6561}. \tag{24}$$

Table 4
Improvement factor for non-dimensional stiffness for pinned topologies compared to unpinned topologies

s	Stiffness model	$l=0$	$l=\infty$
0	1	9	11/7
	2	9	1
	3	9	1
1/4	1	∞	23/19
	2	∞	1
	3	∞	1
1	1	3	7
	2	3	3
	3	3	3

For $s = 1/4$ we get

$$S^1 = \frac{8}{l^2}\frac{l^4+9l^2+8}{19l^4+183l^2+192}, \tag{25}$$

$$S^2 = \frac{16}{l^3}\frac{l^6+\left(4+(l^2+16)^{3/2}\right)l^3+4(l^2+16)^{3/2}}{9l^6+\left(44+10(l^2+16)^{3/2}\right)l^3+48(l^2+16)^{3/2}}, \tag{26}$$

$$S^3 = \frac{128}{l^4}\frac{(l^4+16l^2+128)(l^4+16)}{19l^8+320l^6+2928l^4+6144l^2+49152}. \tag{27}$$

Finally, for $s = 1$ we get

$$S^1 = \frac{2}{l^2+1}, \tag{28}$$

$$S^2 = \frac{2}{l^3+1}, \tag{29}$$

$$S^3 = \frac{2}{l^4+1}, \tag{30}$$

which is particularly simple, because equivalent with the result for $n = 1$. The results (22)–(30) are monotonic decreasing functions of l. This also holds for (12)–(14) in the relevant range of s.

For $s = 1$ it is feasible to display the results for the individual tendon stiffness models, as given below:

$$\frac{1}{S^1} = \frac{1}{2}\frac{l^2}{k_3}+\frac{1}{2}\frac{1}{k_0}, \tag{31}$$

$$\frac{1}{S^2} = \frac{1}{2}\frac{l^3}{k_3}+\frac{1}{2}\frac{1}{k_0}, \tag{32}$$

$$\frac{1}{S^3} = \frac{1}{2}\frac{l^4}{k_3}+\frac{1}{2}\frac{1}{k_0}. \tag{33}$$

For the other two values of s the expressions become unwieldy when using individual tendon stiffnesses, so they are not presented.

Normalized stiffness and normalized stiffness-to-mass ratio are computed in the same way as in Section 4.1.1, but due to pinning nodes, for $s = 1$, several diagonal tendons are no longer needed and their material is redistributed, leading to higher normalized stiffness and normalized stiffness-to-mass. Furthermore, for stiffness model 3, where infinitesimal short tendons still use the same constant amount of tendon material, additional tendons can be taken out of the structure without influencing stiffness, reducing the amount of material and giving higher normalized stiffness and normalized stiffness-to-mass for all class 2 and class 3 structures.

4.2. Stiffness graphs

When looking at the results for a single value of the slenderness ratio, here $l = 3$, it is easier to see the tendencies in the results as function of s. These results are gathered in Fig. 5 and are for the three stiffness models ($k^{\alpha}, \alpha = 1, 2, 3$), five different topologies (2 class 1 and 3 class 2 or 3 topologies), and represent non-

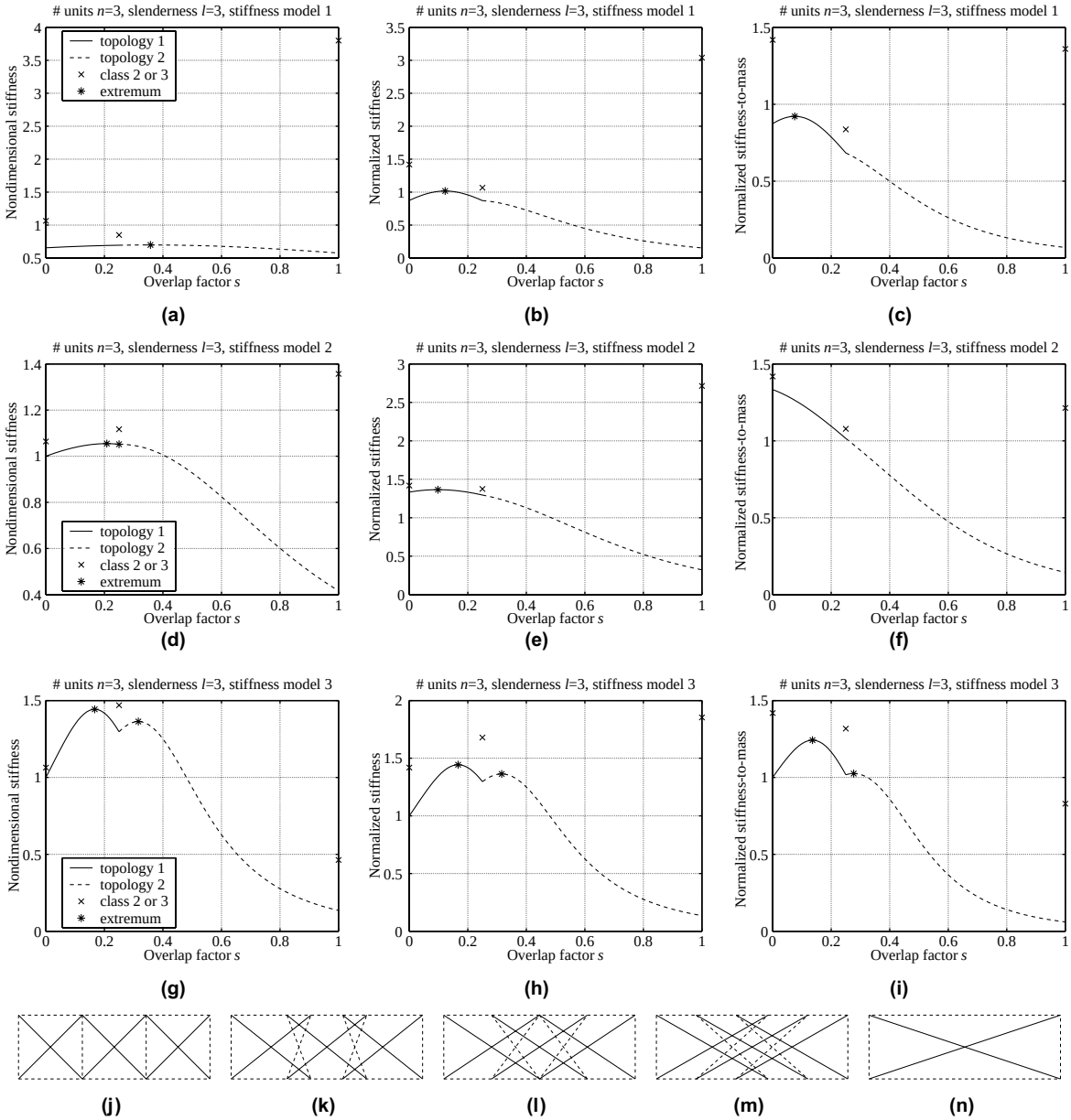

Fig. 5. Results for stiffness (left), normalized stiffness (middle), and normalized stiffness-to-mass (right): upper: equal stiffness; middle: equal cross-sectional area; lower: equal volume; bottom: sketches of topologies, (j), (l), and (n) have pinned common nodes and their data is indicated with an "×" in the graphs; extrema are indicated with a "∗".

dimensional stiffness, normalized stiffness, and normalized stiffness-to-mass ratio as function of overlap. Included in Fig. 5 are sketches of the relevant topologies, for $s = 0$ (Fig. 5(j)), $s = 1/8$ (Fig. 5(k)), $s = 1/4$ (Fig. 5(l)), $s = 3/8$ (Fig. 5(m)), and $s = 1$ (Fig. 5(n)). Note that the results are scaled so for stiffness model 3 and $s = 0$ the results are unity. In the figure, the results for class 2 and 3 topologies are indicated by an "×" and extrema are indicated by a "*".

For comparison and to get insight in their appropriateness, we also include the results for the three stiffness models in a single graph, for several values of l, in Fig. 6.

The results in Fig. 6 can be compared to the results in Fig. 7 where normalized stiffness is given as function of overlap s when the individual tendon stiffnesses k_i are chosen optimally. This results was obtained from the equations in Section 4.1.2, by requiring a stationary point for the stiffness as function of s. This requirement results in up to 16 solutions, in which each of the expressions for k_i is a complicated function of s, when l is fixed. Requiring a physical meaningful solution, i.e., k_i, $i = 0, \ldots, 4$, real and non-negative, leads to a unique solution, however.

The optimal values for k_i, $i = 0, \ldots, 4$, are given in Figs. 8–10. The first set of figures shows the results expressed in the k_i belonging to stiffness model 3, so related to the volume of the tendons. The result are scaled so the sum of the tendon volumes is unity. Note that some tendons get a volume of 0 for $s = 0$, $s = 1/4$, or $s = 1$. The second set gives the corresponding cross-sectional areas, i.e., the volume divided by the tendon length, or the results expressed in the k_i belonging to stiffness model 2. The last set represents the results for tendon stiffness itself, i.e., the stiffness according to stiffness model 1 or the volume divided by the tendon length squared. It is easy to see that for some tendons the optimal stiffness goes to ∞. This is physically possible because the corresponding lengths go to 0.

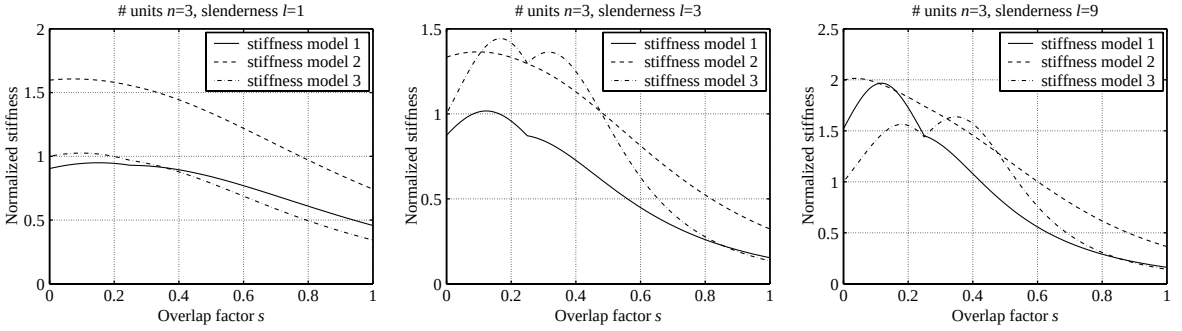

Fig. 6. Comparison of normalized stiffness for the three stiffness models and for several values of l.

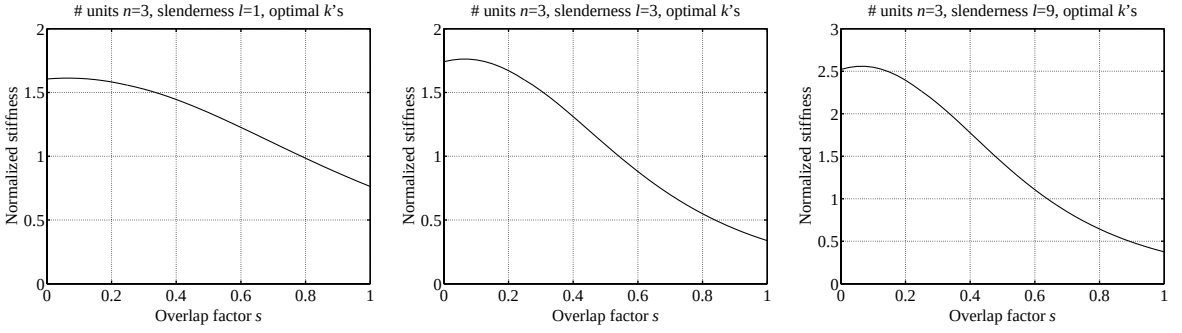

Fig. 7. Normalized stiffness for the optimal choice of tendon stiffnesses k_i, $i = 0, \ldots, 4$, and for several values of l.

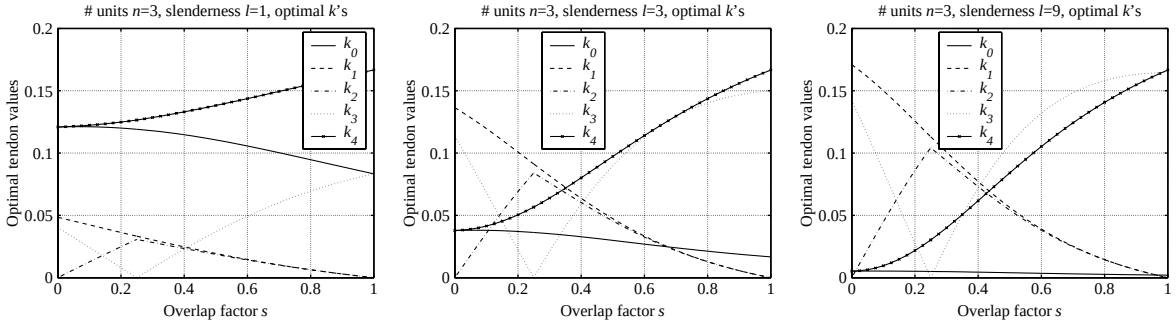

Fig. 8. Tendon stiffnesses k_i, $i = 0, \ldots, 4$, for stiffness model 3, proportional to amount of tendon material, for maximal structural stiffness, for several values of l.

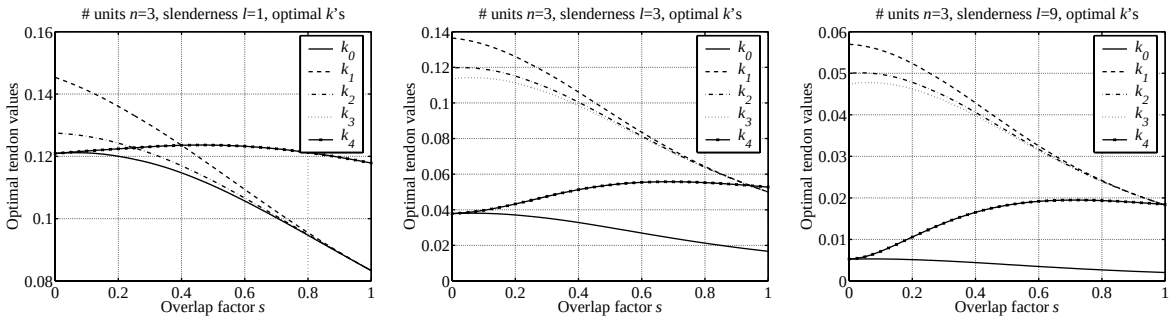

Fig. 9. Tendon stiffnesses k_i, $i = 0, \ldots, 4$, for stiffness model 2, proportional to tendon cross-sectional area, for maximal structural stiffness, for several values of l.

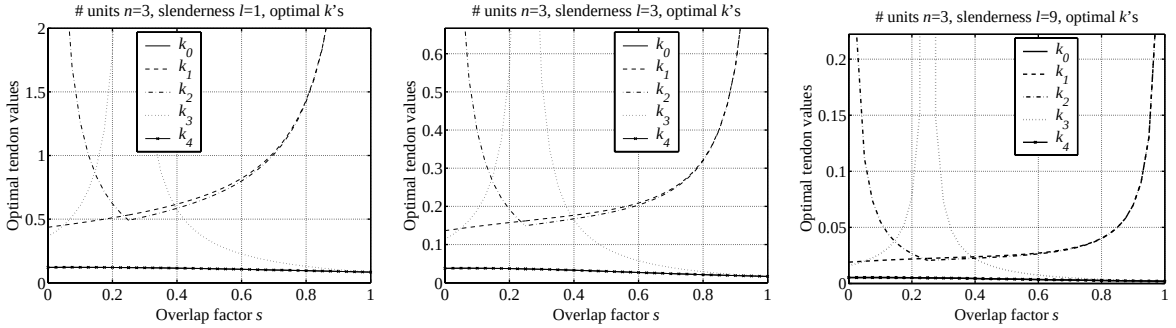

Fig. 10. Tendon stiffnesses k_i, $i = 0, \ldots, 4$, for stiffness model 1, proportional to tendon stiffness, for maximal structural stiffness, for several values of l.

To assess the influence of the number of units, the results for normalized stiffness and structures with $n = 3$ and $n = 9$ units are presented in Fig. 11. Note that the unit overlap factor $\bar{s}$ is used to enable a unified display and comparison of the results.

To validate the results obtained with the symbolic approach, a numerical code was used that takes account of nonlinear geometries (Levy and Spillers, 1995), i.e., that does not use the infinitesimal small

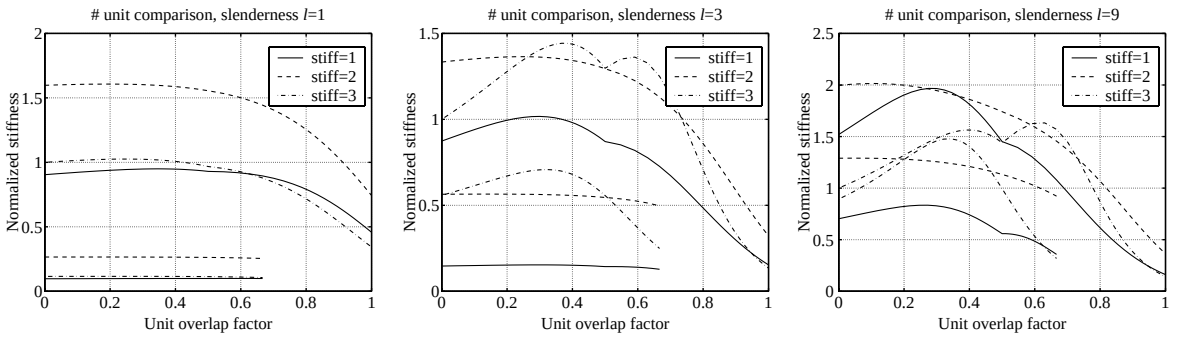

Fig. 11. Normalized stiffness for number of units equal to $n = 3$ (lines continue to $\bar{s} = 1$) and $n = 9$ (lines continue to $\bar{s} = 2/3$), for several stiffness models and for several values of l.

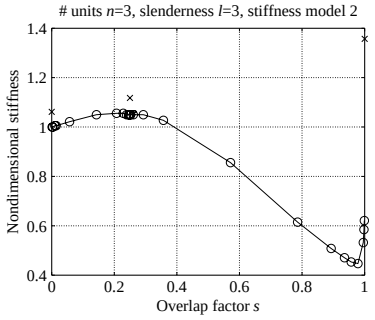

Fig. 12. Results of nonlinear stiffness computation: equal cross-sectional area, structures with pinned joints are indicated with an "×".

deformation assumption of the linear analysis. These results also indicate the effect of short tendons on the stiffness near the geometries that allow pinning.

The result of the numerical computation is presented in Fig. 12. Data is only presented for stiffness model 2, the only one that was supported directly by the code used. This result is to be compared with Fig. 5(d) for the symbolic computation. The computed displacements for values of s close to $s = 0$, $s = 1/4$, and $s = 1$ are sensitive to the load magnitude, due to the dominance of nonlinear effects for these values of s.

5. Discussion

5.1. Results

The discussion of the results is organized in terms of the factors that influence stiffness and related properties. They are the overlap factor s, the slenderness l, the uniform stiffness models, the optimal values of k_i for the individual stiffness models, the number of units n, and the effect of nonlinearities.

5.1.1. Influence of s for 3 stiffness models

Assuming a constant stiffness model with $k_i = k$ (Fig. 5(a)–(c)) the three-unit class 3 tensegrity truss (100% overlap of units, yielding $s = 1$, Fig. 5(n)) is the most stiff (Fig. 5(a)), mainly due to a considerable

amount of tendon material used. When this is accounted for, the normalized stiffness (Fig. 5(b)) is still best for this structure, but the normalized stiffness-to-mass (Fig. 5(c)) is best for the class 2 structure with pinned joints (no overlap of units, yielding $s = 0$, Fig. 5(j)). This is due to the increase in bar mass when s increases, so structures with small s have an advantage for stiffness-to-mass ratio. The third stiffness-to-mass ratio (Fig. 5(c)) is obtained by a class 1 structure with overlap $s = 0.0755$ (Fig. 5(k)). Extrema in the stiffness, normalized stiffness, and normalized stiffness-to-mass ratio are obtained for, respectively, $s = 0.3571$, $s = 0.1227$, and $s = 0.0755$.

Assuming stiffness model 2 with $k_i = EA/l_i$ (Fig. 5(d)–(f)), the class 3 structure with pinned joints in Fig. 5(n) is stiffest, normalized or not, with Fig. 5(l) with $s = 1/4$ second for stiffness and Fig. 5(j) with $s = 0$ second for normalized stiffness, although Fig. 5(k) with $s = 0.0980$ is almost as good. The best normalized stiffness-to-mass ratios are obtained by the class 2 structure in Fig. 5(j) and the class 1 structure in Fig. 5(k), both with $s = 0$. The extrema for stiffness of the class 1 structures occur for $s = 0.2083$ and $s = 1/4$, and for normalized stiffness for $s = 0.0980$.

Assuming stiffness model 3 with $k_i = EV/l_i^2$ (Fig. 5(g)–(i)), the structures Fig. 5(k) with $s = 0.1669$ and Fig. 5(l) with $s = 1/4$ have similar stiffness. The difference with the class 1 tensegrity in Fig. 5(m) for $s = 0.3158$ is not very large, however. For normalized stiffness Fig. 5(n) with $s = 1$ is best, mainly due to the elimination of superfluous tendons. For normalized stiffness-to-mass Fig. 5(j) is best due to the small value of s, but Fig. 5(l) with $s = 1/4$ and Fig. 5(k) with $s = 0.1360$ are not much worse. The extrema for the class 1 structure occur for $s = 0.1669$ and $s = 0.3158$ for (normalized) stiffness and for $s = 0.1360$ and $s = 0.2768$ for normalized stiffness-to-mass.

For class 2 or 3 tensegrities results for $l = 1$ and $l = 9$, Figs. 13 and 14 in Appendix A, show that pinning is especially favorable for small values of l for all stiffness models, but has no advantage for stiffness models 2 and 3 for large values of l, except for $s = 1$ and except for the elimination of superfluous tendons for $s = 1/4$ and/or $s = 1$ influencing normalized stiffness(-to-mass). For large values of l and stiffness model 1 improvements in stiffness are possible by pinning nodes for all 3 class 2 or 3 topologies, see also Table 4.

To summarize, for all three stiffness models class 2 of class 3 topologies with $n = 3$ and $l = 3$, ($s = 1$, $s = 1$, $s = 1/4$ for stiffness and $s = 1$, $s = 1$, $s = 1$ for normalized stiffness, respectively) give better stiffness and normalized stiffness than class 1 topologies. Larger values of s are favored for the normalized stiffness because for $s = 1$ more tendons can be eliminated when pinning joints. Pinning joints is assumed to be a measure without weight penalty. The results for normalized stiffness-to-mass show the same tendencies, but favor smaller s when compared to the results for normalized stiffness due to increasing bar mass for increasing s. Hence a class 2 tensegrity with overlap $s = 0$ is optimal for all stiffness models. The disadvantage of class 2 or 3 is that there are more restrictions when the shape of the structure needs to be changed.

5.1.2. Influence of l

For other slenderness ratios than $l = 3$, the tendencies in the results may be somewhat different, as can be derived from the results in Sections 4.1.1 and 4.1.2 and from Figs. 13 and 14. To see how the previously discussed results have to be modified for different values of slenderness l we look at Fig. 6. For normalized stiffness and class 1 structures this figure shows that stiffness model 2 is most advantageous, except for intermediate values of slenderness l, where stiffness model 3 may be better for certain intervals of s. For large values of l also stiffness model 1 may be sometimes better than model 2, but only on a small interval for s.

Considering class 2 or 3 topologies, for small l the structure in Fig. 5(l) for $s = 1/4$ is favored, because for $l \downarrow 0$ it is the only topology for which the stiffness goes to ∞ (see Table 4), due to a direct load carrying path via rigid bars to the vertical support at the top/left node.

5.1.3. Influence of uniform stiffness models

The best result for class 1 tensegrities, overall, and by an appropriate choice of s, is obtained by stiffness model 2 for small values of l, model 3 is to be preferred for larger values of l on a certain interval for s, while

for even larger values of l model 2 is again preferred. Stiffness model 1 is less appropriate in most cases, mainly due to constant stiffness for short tendons.

A physical explanation for the decline of normalized stiffness for stiffness models 1 and 3 near $s = 0$ and $s = 1/4$ if l is not small is as follows:

model 1: the constant stiffness for short tendons, while a little amount of material could make them very stiff,

model 3: the overly large amount of material for short tendons, while they could be made sufficiently stiff with much less material.

Model 2 seems a reasonable compromise, except perhaps for the cases that none of the tendons is very short or very long.

5.1.4. Influence of individual tendon stiffness

From the results in Figs. 6–10 we can conclude that for small l, stiffness model 2 is nearly optimal. Here, constant cross-sectional area is preferred because vertical and diagonal tendons dominate, have about equal length, and appear similarly in the expressions for stiffness for small l, while the horizontal tendons are quite short, which is not handled well by both stiffness model 1 and 3, as discussed previously. The agreement over a large range of s is due to the dominance of vertical and horizontal tendons, and changing s will only lead to small changes in their length.

For larger l, stiffness model 2 is only close to optimal for large values of s. For smaller values of s none of the uniform tendon stiffness models comes close to the optimal result with individual tendon stiffness. From this we conclude that for small l and/or large s, stiffness model 2 is to be preferred and compares well with individual tendon stiffness, but for larger l and smaller s individual tendon stiffness is to be preferred. In those cases also one of the other uniform tendon stiffness models can give better results.

5.1.5. Influence of n

When relating the number of units, n, to the slenderness ratio, see Fig. 11, we see that a small number of units is preferred, especially for small values of l. For shape control, an application where the number of nodal points is sometimes prescribed, class 1 structures may be preferred, because for a given number of nodal points less units are needed (n is smaller, so stiffness increases). When l becomes much larger than $l = 9$ (results not presented), for stiffness model 3 it becomes true that a number of units n greater than 3 is preferred for the normalized stiffness-to-mass ratio.

5.1.6. Influence of nonlinearities

Comparing the results for symbolic and numerical computations, Figs. 5(d) and 12, we see that the results are mostly in agreement, validating the computations. Only around $s = 0$, $s = 1/4$, and $s = 1$ some differences are to be seen.

In a nonlinear analysis a single tendon with length 0 would pin a common node and therefore the results for cases without common nodes would give higher values of stiffness around $s = 0$, $s = 1/4$, and $s = 1$ than presented in Fig. 5 for a linear analysis, although this depends on the load magnitude. In other words, the lines in Fig. 5 representing stiffness would be smoothly connected to the $\times$-signs when using a nonlinear version of the equilibrium conditions.

This reasoning is verified only partly by Fig. 12, where this smooth trend is only visible around $s = 1$, but not around $s = 0$ and $s = 1/4$. One explanation is the small magnitude of the load that was chosen to compute the stiffness data. From this can be concluded that the effect described is not very large, at least not for small values of the load. We have to remark that numerical computation for values of s very close to $s = 0$,

$s = 1/4$, and $s = 1$ was difficult, due to easy triggering of buckling and snap-through phenomena when pre-stress was neglected (Sheidaii et al., 2001). The high stiffness of very short tendons may lead to numerical problems, which was also a deterrent to go very close to the desired values of s. This illustrates one of the advantages of a symbolic approach over a numerical one.

5.1.7. Cautionary remarks

It is clear that a simple approach using a linearized model may give conservative stiffness results, that is, the real stiffness might be higher. On the other hand, the boundary conditions imply a rigid support and the bars are assumed to be inelastic, which leads to an over estimation of the stiffness. Therefore, for a real structure stiffness slightly above or below the results presented can be expected.

5.2. Conclusion

This paper characterizes, in explicit analytical form and in corresponding graphs, the normalized stiffness and normalized stiffness-to-mass ratio of planar tensegrity trusses composed of $n = 3$ units in detail, and of trusses composed of up to $n = 256$ units in summary.

The symbolic approach is useful because it provides detailed analytical information, even for large scale problems, see also De Jager and Skelton (2004). Furthermore, the approach is not hampered by numerical ill-conditioning and easily allows for the computation of limit cases. Due to the complexity of symbolic computation, limiting both the size of the structure analyzed and the kind of analysis, the approach will be complementary to other approaches.

Information is provided about the preference for different topologies and geometries. The results of the analysis are profitable for the design of very complex systems, when the design is nested, leading to tensegrity fractals (Skelton et al., 2002) or repetitive structures.

A disadvantage of the approach in this paper is the stylized problem formulation, where only a linear compliance analysis is performed. Failure conditions are not included, nor geometric or material nonlinearities. This is not a big disadvantage. Most design optimizations are carried out based on a linear analysis. Other properties, like stability of the elastic equilibrium, that cannot be assessed by a linear problem formulation, are checked a posteriori. It seems also possible to redress this disadvantage, see Section 5.3.

From the problem used to illustrate the symbolic approach, we note that tensegrity trusses with only class 1 nodes do not excel at stiffness, but have controllability advantages, as reported earlier. In general, structures where some of the nodes are pinned, allowing less freedom to move, are preferred to get a low compliance. This is not a big argument against class 1 tensegrities. Tensegrity structures are most useful when changes in shape are required, and then class 2 nodes restrict the kinematics of the system, so they will not be preferred anyway. Discarding the class 2 or 3 topologies and looking at the second stiffness model, it can be seen that an overlap between $s = 0$ and $s = 1/4$ is optimal for normalized stiffness, so a distinct topology is preferred, while the choice for s depends on l but is not very critical. Regarding stiffness-to-mass, a no overlap solution, $s = 0$, is preferred.

5.3. Recommendations

Extension of the symbolic approach seems feasible and worthwhile. The approach can be expanded to more elaborate set-ups with less assumptions on the problem formulation. A straightforward possibility is to formulate the full nonlinear equilibrium conditions, taking care of geometric and material nonlinearities, and of pre-stress. This can be done, but will give a complicated set of nonlinear equations in the DOF, for which no solution can be expected symbolically. It is, however, straightforward to compute the Jacobian of this set of equations with respect to the DOF, and then proceed with the approach outlined in this paper.

This can be done for several levels of the load or pre-stress, so the influence of nonlinearity on compliance is accessible and can be studied.

It seems possible to assess properties like global stability or failure conditions, e.g., yield and local buckling, only for small scale problems, where the solution can be exact, of for larger scale problems, where the

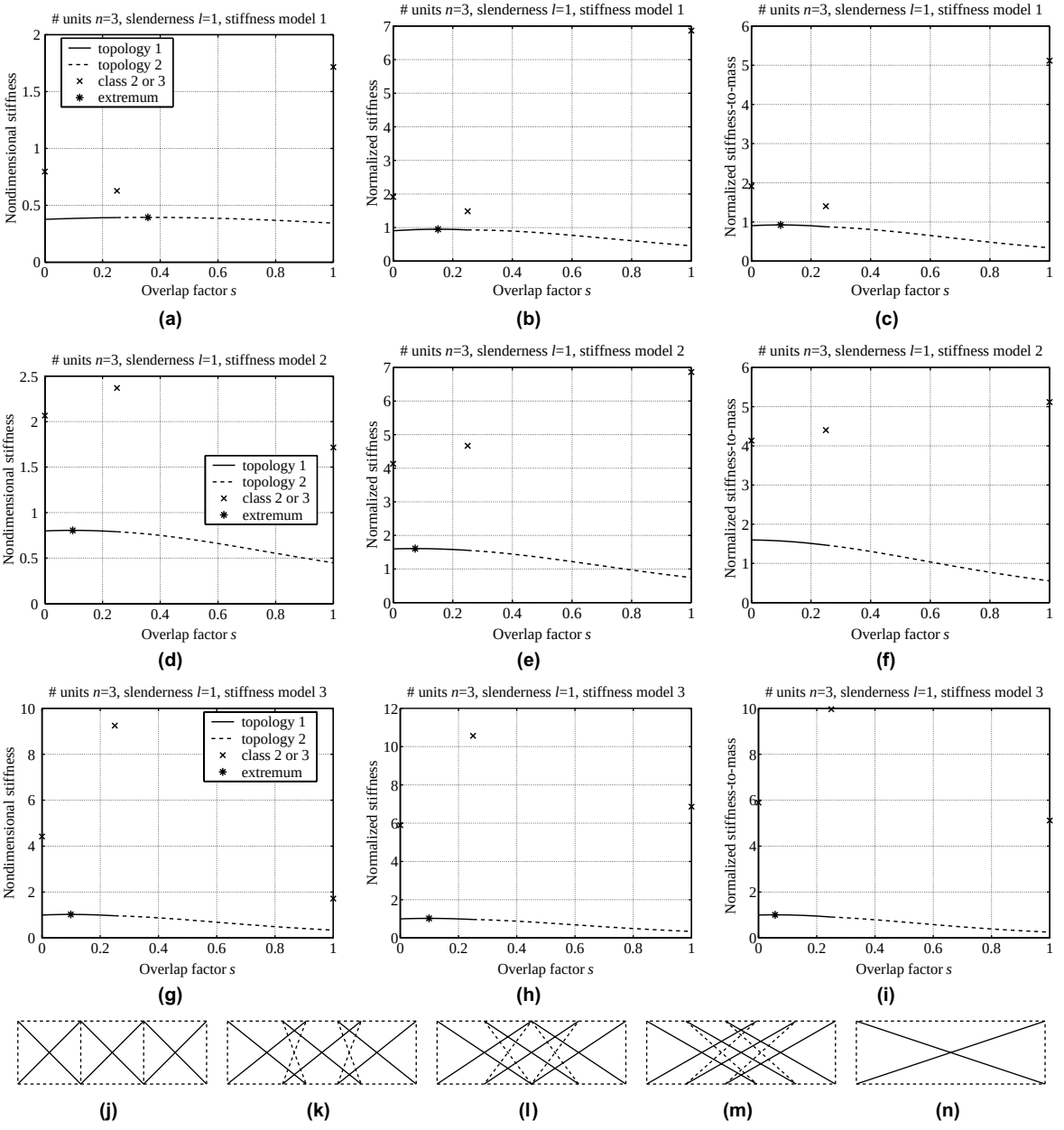

Fig. 13. Results for stiffness (left), normalized stiffness (middle), and normalized stiffness-to-mass (right): upper: equal stiffness; middle: equal cross-sectional area; lower: equal volume; bottom: sketches of topologies, (j), (l), and (n) have pinned common nodes and their data is indicated with an "×" in the graphs; extrema are indicated with a "*".

analysis can be based on repeated linearization and path-following techniques. Another method is to approximate the buckling conditions, like in Kočvara (2002). Other approaches that can defy shortcomings of the symbolic approach, like free material design (Bendsøe, 1989, 1995), or optimal truss topology design based on elimination techniques (Ben-Tal and Nemirovski, 1997; Jarre et al., 1998), may have more appeal for complicated, non-repetitive or wide reach, structures, however.

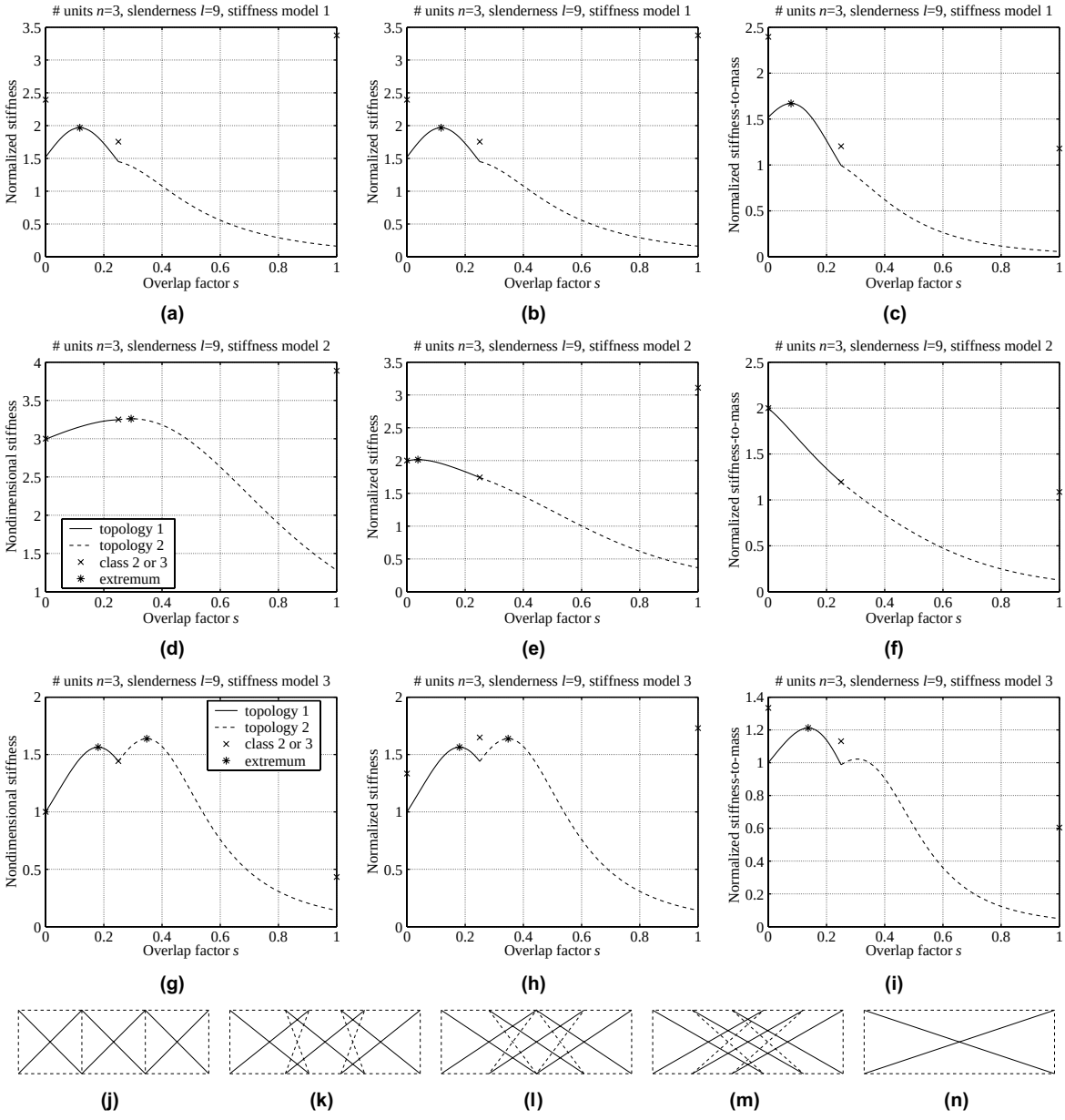

Fig. 14. Results for stiffness (left), normalized stiffness (middle), and normalized stiffness-to-mass (right): upper: equal stiffness; middle: equal cross-sectional area; lower: equal volume; bottom: sketches of topologies, (j), (l), and (n) have pinned common nodes and their data is indicated with an "×" in the graphs; extrema are indicated with a "*".

It is clear that full control of the length of all tendons makes it possible to make the structure infinitely stiff. The limiting process, when the stiffness tends to infinity, is also amenable to a symbolic approach, and avoids the numerical problems that can be expected when the member stiffness becomes very high, as encountered with other approaches. Dynamically changing tendon lengths may be a promising way for designing better, i.e., stiffer, tensegrity structures.

To include shape changing capabilities in the analysis will require some form of feedforward (steering) or feedback control. For optimal design we may only require a criterion that is related to the ease of changing the shape, and to the degree it is possible to change shape. There are some restrictions with respect to shape changes. One of them is the requirement of integrity, or stability, of the structure. Not all configurations are equally versatile in morphing itself to other shapes and, during this process, keep their stability properties at all intermediate configurations. Design optimization with respect to morphing capabilities with stability constraints seems therefore worthwhile, but appears to be an entirely new problem.

Appendix A. Additional results

Full results for $l = 1$ (Fig. 13) and $l = 9$ (Fig. 14), like Fig. 5.

Note that pinning nodes is especially beneficial for small values of l, but not for larger values of l for stiffness models 2 and 3, except for the $s = 1$ case.

References

Ashby, M.F., 1991. Materials and shape. Acta Metall. Mater. 39 (6), 1025–1039.

Babuška, I., Sauter, S.A., 2004. Algebraic algorithms for the analysis of mechanical trusses. Math. Comput. 73 (248), 1601–1622.

Bayat, J., Crane III, C.D., 2004. Closed-form equilibrium analysis of a planar tensegrity structure. In: Proc. 9th Int. Symp. on Advances in Robot Kinematics. Sestri Levante.

Ben-Tal, A., Nemirovski, A., 1997. Robust truss topology design via semidefinite programming. SIAM J. Optim. 7 (4), 991–1016.

Ben-Tal, B., Kočvara, M., Zowe, J., 1993. Two nonsmooth methods for simultaneous geometry and topology design of trusses. In: Bendsøe, Soares (Eds.), Topology Optimization of Structures. Kluwer Academic Publishers, pp. 31–42.

Bendsøe, M.P., 1989. Optimal shape design as a material distribution problem. Struct. Optim. 1, 193–202.

Bendsøe, M.P., 1995. Optimization of Structural Topology, Shape and Material. Springer-Verlag, Berlin.

Connelly, R., Back, A., 1998. Mathematics and tensegrity. Am. Sci. 86 (2), 142–151.

De Jager, B., Skelton, R.E., 2004. Symbolic stiffness optimization of planar tensegrity structures. J. Intell. Mater. Syst. Struct. 15 (3), 181–193.

Fest, E., Shea, K., Domer, B., Smith, I.F.C., 2003. Adjustable tensegrity structures. J. Struct. Engrg. 129 (4), 515–526.

Guest, S.D., Hutchinson, J.W., 2003. On the determinacy of repetitive structures. J. Mech. Phys. Solids 51 (3), 383–391.

Hanaor, A., 1988. Prestressed pin-jointed structures–flexibility analysis and prestress design. Comput. Struct. 28 (6), 757–769.

Ingber, D.E., 2003. Tensegrity I. Cell structure and hierarchical systems biology. J. Cell Sci. 116 (7), 1157–1173.

Jarre, F., Kočvara, M., Zowe, J., 1998. Optimal truss design by interior-point methods. SIAM J. Opt. 8 (4), 1084–1107.

Karpov, E.G., Stephen, N.G., Dorofeev, D.L., 2002. On static analysis of finite repetitive structures by discrete Fourier transform. Int. J. Solids Struct. 39 (16), 4291–4310.

Klimke, H., Stephan, S., Essrich, R., 2004. Fertigung und Montage des Messeturms in Rostock. Stahlbau 73 (2), 74–79.

Kočvara, M., 2002. On the modelling and solving of the truss design problem with global stability constraints. Struct. Multidisc. Optim. 23 (3), 189–203.

Lakes, R., 1993. Materials with structural hierarchy. Nature 361 (6412), 511–515.

Leff, L., Yun, D.Y.Y., 1991. The symbolic finite element analysis system. Comput. Struct. 41 (2), 227–231.

Levy, R., Spillers, W.R., 1995. Analysis of Geometrically Nonlinear Structures. Chapman & Hall, New York.

Liapi, K.A., Kim, J., 2004. A parametric approach to the design of vaulted tensegrity networks. Int. J. Archit. Comput. 2 (2), 245–262.

Masic, M., 2004. Design, optimization, and control of tensegrity structures. Ph.D. thesis. University of California San Diego, Department of MAE, La Jolla, CA, USA.

Maxwell, J.C., 1890. The Scientific Papers of James Clerk Maxwell. Dover, New York.

McEachen, M.E., Trautt, T.A., Murphy, D.M., 2004. SALT: Second-order augmentation of lattice trusses. In: Proc. 45th Structures, Structural Dynamics & Materials Conf. AIAA/ASME/ASCE/AMS/ASC. Palm Springs, CA. Paper AIAA-2004-1729.

Motro, R., Raducanu, V., 2003. Tensegrity systems. Int. J. Space Struct. 18 (2), 77–84.
Murakami, H., Nishimura, Y., 2001. Static and dynamic characterization of some tensegrity modules. Trans. ASME J. Appl. Mech. 68 (1), 19–27.
Murphey, T.W., Hinkle, J.D., 2003. Some performance trends in hierarchical truss structures. In: Proc. 44th Structures, Structural Dynamics and Materials Conf. AIAA/ASME/ASCE/AMS/ASC. Norfolk, VA. Paper AIAA-2003-1903.
Noor, A.K., 1988. Continuum modeling for repetitive lattice structures. Appl. Mech. Rev. 41 (7), 285–296, Reprint No. AMR039, see also NASA TP2767.
Noor, A.K., Andersen, C.M., 1979. Computerized symbolic manipulation in structural mechanics—progress and potential. Comput. Struct. 10 (1–2), 95–118.
Oppenheim, I.J., Williams, W.O., 2000. Geometric effects in an elastic tensegrity structure. J. Elasticity 59 (1–3), 51–65.
Pavlović, M.N., 2003. Symbolic computation in structural engineering. Comput. Struct. 81 (22–23), 2121–2136.
Pellegrino, S., 1990. Analysis of prestressed mechanisms. Int. J. Solids Struct. 26 (12), 1329–1350.
Pellegrino, S., Calladine, C.R., 1986. Matrix analysis of statically and kinematically indeterminate frameworks. Int. J. Solids Struct. 22 (4), 409–428.
Scruggs, J.T., Iwan, W.D., 2003. Control of a civil structure using an electric machine with semiactive capability. J. Struct. Engrg. 129 (7), 951–959.
Sheidaii, M.R., Parke, G.A.R., Abedi, K., Behravesh, A., 2001. Dynamic snap-through buckling of truss-type structures. Int. J. Space Struct. 16 (2), 85–93.
Skelton, R.E., 2002. Structural systems: a marriage of structural engineering and system science. J. Struct. Control 9 (2), 113–133.
Skelton, R.E., Helton, J.W., Adhikari, R., Pinaud, J.-P., Chan, W., 2002. An introduction to the mechanics of tensegrity structures. In: Nwokah, O.D.I., Hurmuzlu, Y. (Eds.), The Mechanical Systems Design Handbook: Modeling, Measurement, and Control. CRC Press, Boca Raton, pp. 315–388 (Chapter 17).
Snelson, K., 1996. Snelson on the tensegrity invention. Int. J. Space Struct. 11 (1–2), 43–48.
Sultan, C., Skelton, R., 2003. Deployment of tensegrity structures. Int. J. Solids Struct. 40 (18), 4637–4657.
Williamson, D., Skelton, R.E., Han, J., 2003. Equilibrium conditions of a tensegrity structure. Int. J. Solids Struct. 40 (23), 6347–6367.